INTERNATIONAL JOURNAL FOR NUMERICAL METHODS IN FLUIDS
Int. J. Numer. Meth. Fluids 2003; **41**:209–223 (DOI: 10.1002/fld.437)

Approximate simulation of stratospheric flow from aircraft data

Mayer Humi*

Department of Mathematical Sciences, Worcester Polytechnic Institute, Worcester, MA 01609, U.S.A.

SUMMARY

We show how stratospheric data collected by an aircraft along its flight path can be used to initialize steady state approximate simulations of the stratospheric flow. To this end we reformulate the initial value problem for Boussinesq equations as a large system of stiff ordinary differential equations (using the method of lines). Initial conditions for this system are derived from the aircraft data. As a result we are able to compute the Brunt–Vaisala frequency, Richardson number and the vorticity in the vicinity of the flight path. Copyright © 2003 John Wiley & Sons, Ltd.

1. INTRODUCTION

Several scientific missions were undertaken in the last two decades to collect data about the atmospheric flow (and trace gases) in the stratosphere or the upper troposphere [1–3]. This data is important from a fundamental scientific point of view (e.g. the understanding of natural turbulence phenomena [4–7]) as well as a practical point of view (e.g. the determination of atmospheric structure constants [8, 9]).

In the past this data was collected by high flying airplanes equipped with one meteorological probe. This probe sampled the basic flow variables (viz. velocity, pressure, temperature and trace gas concentrations) along the flight path. However it was impossible to use this data to compute several important characteristics of the flow such as the Brunt–Vaisala frequency, the Richardson number or to initiate simulations of the flow in the vicinity of the flight path (to determine the vorticity field and the large scale structure of the flow).

In an attempt to overcome some of these difficulties a special purpose airplane was equipped with three probes (on the wings and tail) to collect data about the atmospheric flow at heights of about 10 km [3]. (This plane was named 'EGRETT'.) The new data collected by this 'platform' enabled us to compute the flow gradients along the flight path. However it does not provide the data needed to compute the initial and boundary conditions to initiate 3-D simulations of the flow. In fact we do not have at the present (nor in the foreseeable future) the technological means to collect the data needed for such high resolution

* Correspondence to: M. Humi, Department of Mathematical Sciences, Worcester Polytechnic Institute, Worcester, MA 0l609, U.S.A.

Received 10 November 2001
Revised 9 September 2002

simulations. It is the objective of this paper to show however that this data can be used to initiate an 'approximate' simulation of the atmospheric flow around the plane flight path (up to a distance of a few hundred metres). This will enable us to compute at least an estimate of the quantities that were impossible to calculate using the data collected by previous expeditions.

To achieve these objectives we introduce an approximate model for the atmospheric flow under consideration. With these approximations we are able to simulate two dimensional cross-sections of the flow by using the steady state Boussinesq equations [10, 11]. We then demonstrate that this system of partial differential equations (PDES) can be reformulated as a large stiff system of ordinary differential equations (ODES) using the method of lines [12, 13]. Initial data for the solution of this system of ODES can be extracted from the data collected along the flight path coupled with appropriate data decomposition technique (to extract the mean flow from the waves and the turbulence fluctuations). The ensuing simulations for the atmospheric flow (in the vicinity of the plane flight path) enable us to obtain insights about its nature, its large scale structure and the 'numbers' that characterize it.

We wish to note at this juncture that the method of lines has been used in many applications. However we believe that its application to the steady state Boussinesq equations which are being reformulated so that one of the spatial co-ordinates is used as 'time' (as is being done in this paper) did not appear in the literature before. Also we want to emphasize again that the simulations and the results reported in this paper are only approximate and should be viewed within this framework. It is hoped however that the methodology used in this context will be found to be useful in other situations where there is not enough data to initiate a full simulation of the governing equations.

The plan of the paper is as follows. In Section 2 we enumerate and discuss the approximations that we have to impose in order to derive model equations that can be simulated using the flight data. In Section 3 we reformulate these equations as a large system of ODEs using the method of lines. Section 4 describes the methodology used to extract the initial data necessary for the simulation from the flight data. Finally in Section 5 we present and discuss the simulation results and end with some conclusions in Section 6.

2. APPROXIMATE MODEL FOR THE FLOW

In this paper we shall use the data collected by the Egrett on 6 August 1999 over Australia. The meteorological data was sampled at constant time frequency of about 55.1 Hz (0.017 s). The airplane speed was about 100 m/s and during the flight segment under consideration the plane was flying in a straight line (which we take as the x-axis) at a constant height of about 9600 m with no clouds in the flight path. The flight time interval during which the data was collected was about $\frac{1}{2}$ hour.

Using this input it follows that an appropriate model equations that govern the flow for short distances from the plane are given by the time dependent 3-D Boussinesq equations [4, 5]. In non-dimensional form these equations are

$$\nabla \cdot \mathbf{u} = 0 \tag{1}$$

$$\frac{\partial \mathbf{u}}{\partial t} + (\mathbf{u}\cdot\nabla)\mathbf{u} = -\nabla p + \frac{1}{Re}\nabla^2\mathbf{u} + \frac{1}{Fr}\theta\mathbf{k} \tag{2}$$

$$\frac{\partial \theta}{\partial t} + (\mathbf{u}\cdot\nabla)\theta = \frac{1}{RePr}\nabla^2\theta \tag{3}$$

Here $\mathbf{u} = (u, v, w)$ is the flow velocity, p is the pressure, θ the potential temperature and Re, Fr, Pr are the Reynold's, Froude's and Prandtl's numbers, respectively.

It is easy to see however that the data collected by the aircraft is not sufficient to initiate a 3-D simulation of these equations. We must introduce therefore some simplifying approximations under which the available data is sufficient to provide us with the necessary initial conditions. To this end we shall restrict ourselves to two-dimensional simulations of the flow either in the x–y (horizontal) plane or the x–z (vertical) plane and introduce the following assumptions:

A. The time duration of the measurements is short compared to other (time dependent) processes taking place. Accordingly we assume that for this duration the flow is in a quasi-time independent state. Consequently we make the approximation that the measurements are taken simultaneously and use the steady state Boussinesq equations in our simulations.
   To justify this approximation we invoke Taylor (frozen wave) hypothesis which is commonly used in the analysis of meteorological time series [10]. According to this hypothesis we can treat the data collected along the flight path as equivalent to one collected at one space point at different times. It follows then that we can use these time series to compute the (time) rate of change of the wind W (or its components). Using standard estimation techniques we find that $\langle \partial W/\partial t\rangle \cong 2\times 10^{-3}\mathrm{m/s}^2$. Since the time interval for the measurements is ≈ 2000 s we estimate the temporal change in W during this time interval to be ≈ 4 m/s or (since $\langle W\rangle \cong 81$ m/s) a relative change of 5%.
B. It is well known from other studies that the stratospheric flow is almost two dimensional. This is confirmed by our data where we have $|w| \ll |u|, |v|$, $|\partial w/\partial x| \ll 1$, $|\partial w/\partial y| \ll 1$. Hence the third momentum equation (Equation (2) in the z-direction) decouples approximately from the other two momentum equations and we can simulate the remaining equations in the x–y plane by treating u, v, θ as functions of x–y only.
C. The stratospheric flow in the vertical x–z plane is (for very short distances along y) independent of y. This is supported by the fact that the wind gradients along y are small compared to those along x. Consequently we can simulate this flow approximately by using 2-D Boussinesq equations.

Among these approximations the last is the most controversial. In fact it is conceptually in conflict with assumption B (where we let $v = v(x, y)$). It should be viewed then as a 0-approximation which enables us to simulate the flow in the x–z plane. We observe however, that to some extent, this assumption is supported *a posteriori* by the results of the simulations in the x–y plane.

3. REFORMULATION OF THE PROBLEM

In this section we reformulate the steady state 2-D Boussinesq equations (for flows in the x–y, x–z planes) as an initial value problem for a (large and stiff) system of

ODEs. As these two flows have somewhat different characteristics we consider them separately.

3.1. The flow in the x–y plane

Under the assumptions made earlier the equations that govern this flow are

$$\frac{\partial u}{\partial x} + \frac{\partial v}{\partial y} = 0 \tag{4}$$

$$u\frac{\partial u}{\partial x} + v\frac{\partial u}{\partial y} = -\frac{\partial p}{\partial x} + \frac{1}{Re}\nabla^2 u \tag{5}$$

$$u\frac{\partial v}{\partial x} + v\frac{\partial u}{\partial y} = -\frac{\partial p}{\partial y} + \frac{1}{Re}\nabla^2 v \tag{6}$$

$$u\frac{\partial \theta}{\partial x} + v\frac{\partial \theta}{\partial y} = \frac{1}{RePr}\nabla^2 \theta \tag{7}$$

We see then that Equation (7) is decoupled from Equations (4)–(6) and can be solved separately. We can also replace Equation (4) by the pressure equation

$$\nabla^2 p = 2\left(\frac{\partial u}{\partial x}\frac{\partial v}{\partial y} - \frac{\partial u}{\partial y}\frac{\partial v}{\partial x}\right) \tag{8}$$

At this point we note that if one derives the equivalent of Equation (8) in three dimensions additional terms on the right hand side of this equation will have to be included. The most important of these is $(1/F_r)(\partial\theta/\partial z)$ which contributes to the stability of the stratosphere. To gauge the variability of this term (in the x–y plane) we used the meteorological data which was collected (during the plane climb) before and after the measurements were made and obtained the following estimates:

$$\frac{\partial \theta}{\partial z}(x=0) \cong -4.29 \times 10^{-3} \text{ degrees/m}$$

$$\frac{\partial \theta}{\partial z}(x=L) \cong -3.27 \times 10^{-3} \text{ degrees/m}$$

(where L is the length of the flight path $\sim 200\,\text{km}$). Thus $\partial\theta/\partial z$ is almost constant in the x–y plane and it can be included in Equation (8) as an additional constant term.

Our objective is to simulate Equations (5), (6), (8) on a rectangle $[0,a]\times[0,b]$ given that the atmospheric data is sampled at equispaced points x_j on $[0,a]$, $j=1,\ldots,n$.

To this end we introduce

$$\mathbf{w} = (w_1,\ldots,w_6) = \left(u, v, p, \frac{\partial u}{\partial y}, \frac{\partial v}{\partial y}, \frac{\partial p}{\partial y}\right) \tag{9}$$

and rewrite Equations (5), (6), (8) as a system.

$$\frac{\partial w_i}{\partial y} = w_{i+3}, \quad i = 1,2,3$$

$$\frac{\partial w_4}{\partial y} = Re\left\{ w_2 w_4 - \frac{1}{Re}\frac{\partial^2 w_1}{\partial x^2} + w_1\frac{\partial w_1}{\partial x} + \frac{\partial w_3}{\partial x}\right\} \tag{10}$$

$$\frac{\partial w_5}{\partial y} = Re\left\{ w_2 w_5 - \frac{1}{Re}\frac{\partial^2 w_2}{\partial x^2} + w_1\frac{\partial w_2}{\partial x} + w_6\right\} \tag{11}$$

$$\frac{\partial w_6}{\partial y} = 2\left\{ w_5\frac{\partial w_1}{\partial x} - w_4\frac{\partial w_2}{\partial x}\right\} - \frac{\partial^2 w_3}{\partial x^2} \tag{12}$$

or for brevity

$$\frac{\partial \mathbf{w}}{\partial y} = \mathbf{F}\left(x, y, \mathbf{w}, \frac{\partial \mathbf{w}}{\partial x}\right) \tag{13}$$

We can convert this to a system of coupled ODEs using the method of lines. In this technique we require the solution of the system only at the points $x = x_j$ and use finite differences to approximate the partial derivatives of $\mathbf{w}$ with respect to x viz.

$$\frac{\mathrm{d}\mathbf{w}}{\mathrm{d}y}(x_j, y) = \tilde{\mathbf{F}}(x_j, y, \mathbf{w}(x_j, y)) \tag{14}$$

We can solve this system for $y\varepsilon[0, b]$ if we can provide the proper initial conditions on $\mathbf{w}$ (This problem will be addressed in the next section).

3.2. *The flow in x–z plane*

Following the same approach as above we take the equations that govern this flow as

$$u\frac{\partial u}{\partial x} + w\frac{\partial u}{\partial z} = -\frac{\partial p}{\partial x} + \frac{1}{Re}\nabla^2 u \tag{15}$$

$$u\frac{\partial w}{\partial x} + w\frac{\partial w}{\partial z} = -\frac{\partial p}{\partial z} + \frac{1}{Re}\nabla^2 w + \frac{1}{Fr}\theta \tag{16}$$

$$u\frac{\partial \theta}{\partial x} + w\frac{\partial \theta}{\partial z} = \frac{1}{RePr}\nabla^2\theta \tag{17}$$

$$\nabla^2 p = 2\left(\frac{\partial u}{\partial x}\frac{\partial w}{\partial z} - \frac{\partial u}{\partial z}\frac{\partial w}{\partial x}\right) + \frac{1}{Fr}\frac{\partial \theta}{\partial z} \tag{18}$$

(All equations are coupled in this case). Introducing

$$\boldsymbol{\chi} = (\chi_1, \ldots, \chi_8) = \left(u, w, p, \theta, \frac{\partial u}{\partial z}, \frac{\partial w}{\partial z}, \frac{\partial p}{\partial z}, \frac{\partial \theta}{\partial z}\right) \tag{19}$$

we can rewrite Equations (15)–(18) in the form:

$$\frac{\partial \boldsymbol{\chi}}{\partial z} = \mathbf{G}\left(x, z, \boldsymbol{\chi}, \frac{\partial \boldsymbol{\chi}}{\partial x}\right) \tag{20}$$

Once again we can convert this to a system of ODEs by the method of lines by using finite differences to approximate the derivatives of $\boldsymbol{\chi}$ in G;

$$\frac{\mathrm{d}\boldsymbol{\chi}(x_j, z)}{\mathrm{d}z} = \tilde{\mathbf{G}}(x_j, z, \boldsymbol{\chi}(x_j, z)) \tag{21}$$

4. INITIAL AND BOUNDARY CONDITIONS

To simulate Equations (14), (21) we must supply initial conditions at $y = 0$ for $\mathbf{w}$ and $z = 0$ for ξ. These initial conditions require the extraction of the mean flow from the data and the computation of the appropriate derivatives of the primitive variables.

To extract the mean flow we detrended the data using the Karahunan–Loeve algorithm [15, 16] (see Appendix A). As a result the original data has been decomposed into mean flow, waves and turbulent residuals. These are denoted by subscript w and primes, respectively).

$$\mathbf{u} = \bar{\mathbf{u}} + \mathbf{u}_{\mathrm{w}} + \mathbf{u}', \quad \theta = \bar{\theta} + \theta_{\mathrm{w}} + \theta', \quad p = \bar{p} + p_{\mathrm{w}} + p' \tag{22}$$

Using this data decomposition we can compute the components of the averaged Reynold's stress tensor and use the Boussinesq–Kolmogorov postulate

$$\bar{\tau}_{ik} = \frac{1}{3} K \delta_{ij} - \nu_{\mathrm{T}} \left(\frac{\partial \bar{u}_i}{\partial x_k} + \frac{\partial \bar{u}_k}{\partial x_i}\right) \tag{23}$$

$$K = \bar{\tau}_{ii} = \bar{\tau}_{11} + \bar{\tau}_{22} + \bar{\tau}_{33} \tag{24}$$

to obtain a value for the turbulent eddy viscosity ν_{T}

$$\nu_{\mathrm{T}} = \frac{\frac{1}{3}K - \bar{\tau}_{11}}{2(\partial \bar{u}/\partial x)} \tag{25}$$

In the simulation we replaced ν by

$$\nu_{\mathrm{eff}} = \nu + \nu_{\mathrm{T}}$$

To compute the derivatives (at each moment at the plane center) along the x-axis we used the fact that for a general function f

$$\hat{f}' = \frac{1}{i\omega} \hat{f} \tag{26}$$

where $\hat{f}$ is the FFT transform of f. Thus to compute $f'(x)$ we divide each term of $\hat{f}$ by the appropriate frequency ω and then use the inverse FFT of the new series to evaluate $f'(x)$.

The derivatives along y and z can be computed using finite differences. For example one can use the central difference formula

$$f'(0,t) = (f_r(t) - f_l(t))/d \tag{27}$$

where $f'(0,t)$ is the derivative at the centre of the plane at time t, d is the distance between the probes and f_r, f_l are the values of the variable f at the right and left probes, respectively.

However it is possible also to compute this derivative by using the data collected at times $t \pm \Delta t$. Using directional derivatives we obtain after some algebra the following 6-point approximation for

$$\frac{\partial f}{\partial y}(0,t) = \frac{1}{2}\left\{ \frac{f_r(0,t) - f_l(0,t)}{d} + \frac{1}{4\Delta x}[f_r(\Delta x, t+\Delta t) - f_r(-\Delta x, t\Delta t) \right. \tag{28}$$

$$\left. + f_l(\Delta x, t+\Delta t) - f_l(-\Delta x, t-\Delta t)] \right\} \tag{29}$$

As we pointed out earlier the 'Egrett' was equipped (for the flight under consideration) with a probe on each wing and one probe on the tail. The probe on the tail was mounted at a different height than the other two probes. Hence the measurements made by this probe combined with those on the wing enable us to compute the vertical derivatives of the meteorological variables. As a check for consistency $\partial w/\partial z$ was computed directly and by the use of the continuity equation.

Besides the initial conditions we need to impose appropriate boundary conditions on all variables at $x = 0, L$ for the simulations in the x–y and x–z planes. Since we have no actual data to accomplish this we imposed zero normal derivatives on all variables at these points. This is justified by the fact that the measured (averaged) gradients of all variables along the flight path are very small.

Finally it is not computationally feasible to use all the grid points that correspond to the original time series (approximately 100 K points) in the simulation. To reduce this number we averaged the data values over each interval of 8 data points to obtain a x-grid of 13355 points with equal spacing of 11.8 m.

5. RESULTS

To perform the simulations discussed in the previous sections we used the 'method of lines' package that was provided to us by Schiesser [12, 13] and the LSODE [14] package from the NETLIB library [17]. In addition for comparison and verification purposes we used the PDECOL package from NETLIB.

The mean flow which is needed to initiate the simulations was obtained from the Karahunen–Loeve decomposition of the data collected in one flight segment by the EGRETT along the flight path on 6 August 1999 at height of about 9600 m. A sample of this initial data (for u) is shown in Figure 1. From this figure it is clear that the mean flow contains some small oscillations. This leads to a stiff system of ODEs which require careful integration by an implicit algorithm and small (variable) step size.

Plates 1 and 2 are contour plots of the speed and pressure in the x–z plane which were obtained from the simulation. They show the vortical structure of the wind and the pressure waves that accompany them. Plate 3 shows that the vorticity field is made of thin intermittent

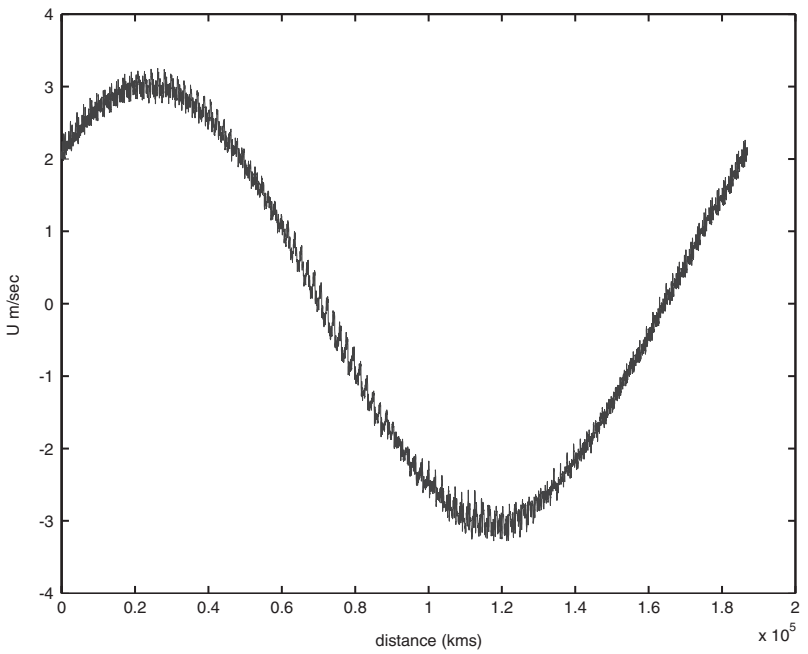

Figure 1. Plot of U mean flow along the flight path.

vertical structures. According to current conceptions [4, 7, 9] these vortical structures decay in time to form thin flat layers of turbulence. We infer then that the plane was transversing an area of strong turbulence. (This fact is corroborated by a spectral analysis of the data.) Plate 4 which is a contour plot of v in the x–y plane demonstrates that assumption C in Section 2 (that v is weakly dependent on y) is justified.

Plate 5 is a contour plot of the Richardson number. It shows that this number varied along the airplane path form positive to negative. This implies that while the flow was stable in some regions of the flight it was unstable in other parts. It will be inappropriate, therefore, to characterize the state of the flow by some averaged value of this number (as is usually done). Figures 2 and 3 show actual cross sections (as a function of height) of the Richardson number at two different values of x along the flight path.

Similarly Figure 4 is a plot of the Brunt–Vaisala frequency along the flight path at 30 m height above the plane. It shows the variability of this frequency along the flight path. Figures 5 and 6 are cross sections (as a function of height) at two different values of x. These plots demonstrate the variable effects of the stratification on the flow at different points along the flight path.

The simulations carried in this paper are approximate. Accordingly it is important to gauge the impact of the different error types on the results. These errors include data noise, numerical integration errors and errors due to the approximations introduced in Section 2.

Based on instrument specifications the data noise should be at a relative error level of 10^{-3}. This is confirmed by the eigenvalues obtained in the Karahunan–Loeve decomposition where the last few eigenvalues (which reflect the noise level in the data) are of order 10^{-3} of the leading eigenvalue (see Figure 7).

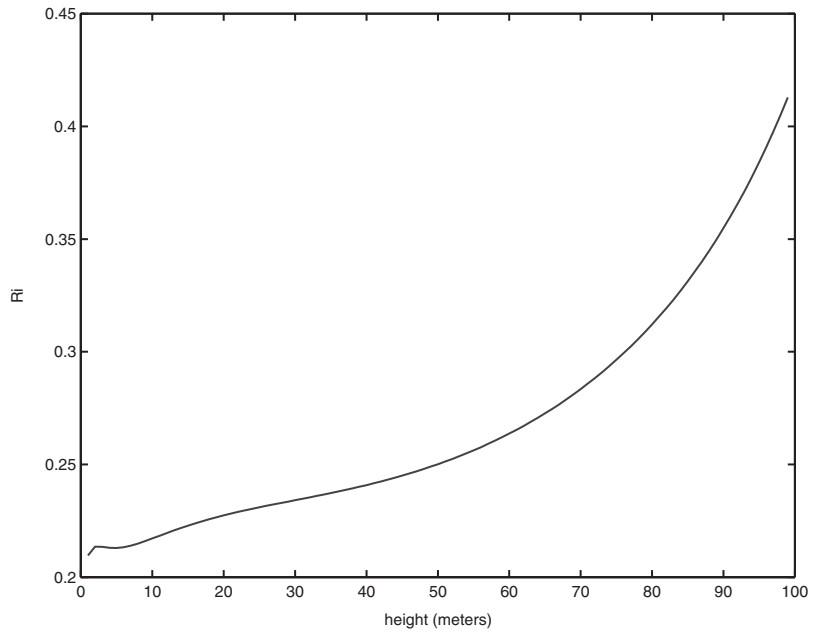

Figure 2. Plot of the Richardson number as a function of the height at flight distance of 18 km.

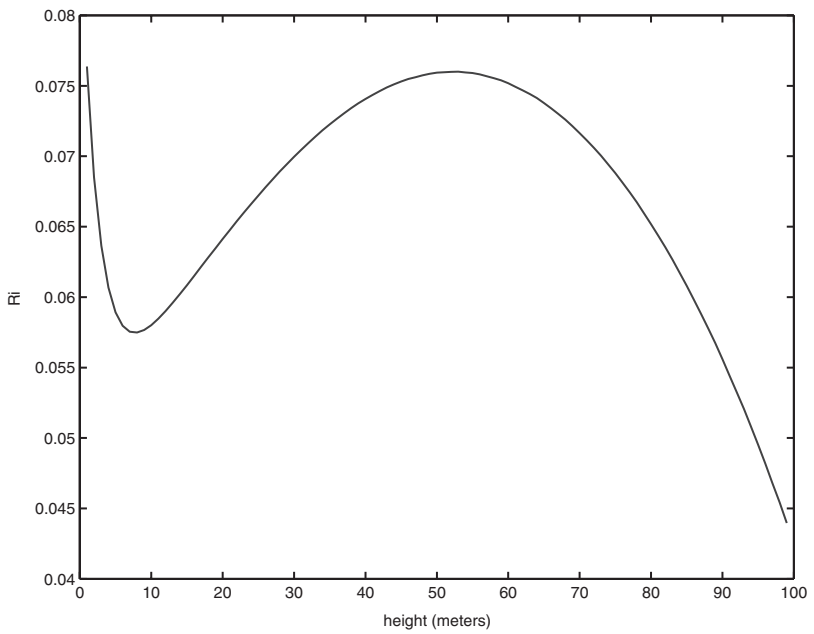

Figure 3. Plot of the Richardson number as a function of the height at flight distance of 85 km.

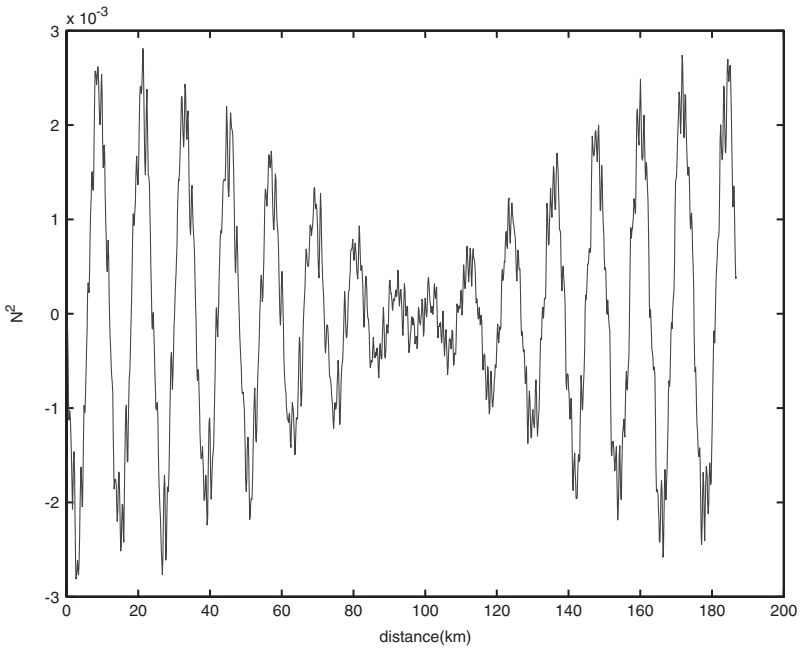

Figure 4. Plot of Brunt–Vaisala frequency (N^2) as a function of the flight distance at 30 m height above the plane.

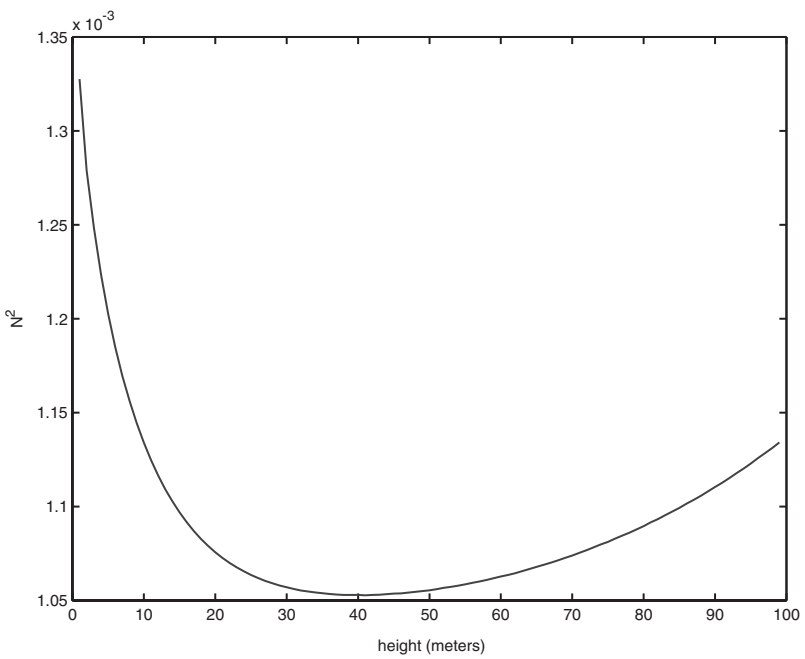

Figure 5. Plot of Brunt–Vaisala frequency (N^2) as a function of the height at flight distance of 35 km.

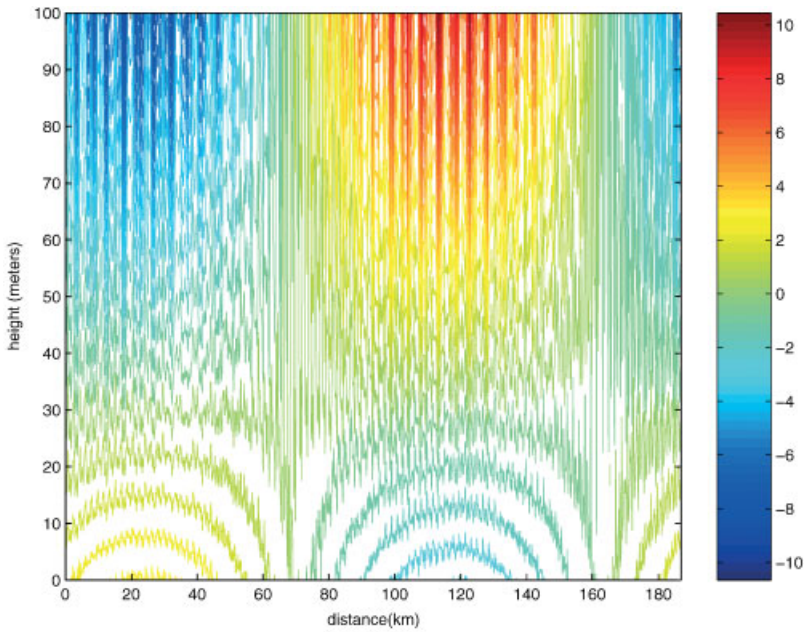

Plate 1. Contour plot of the speed as a function of the flight distance and height (simulation in the x–z plane).

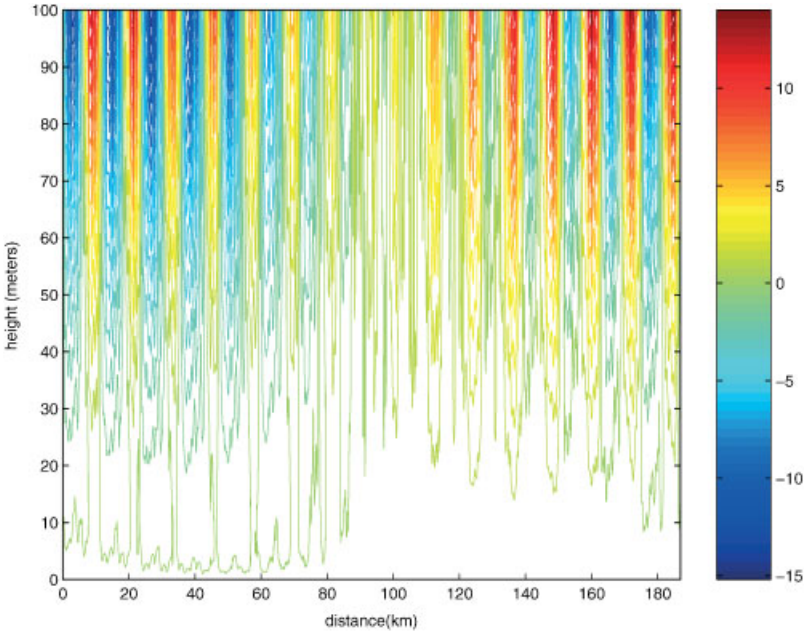

Plate 2. Contour plot of the pressure as a function of the flight distance and height (simulation in the x–z plane).

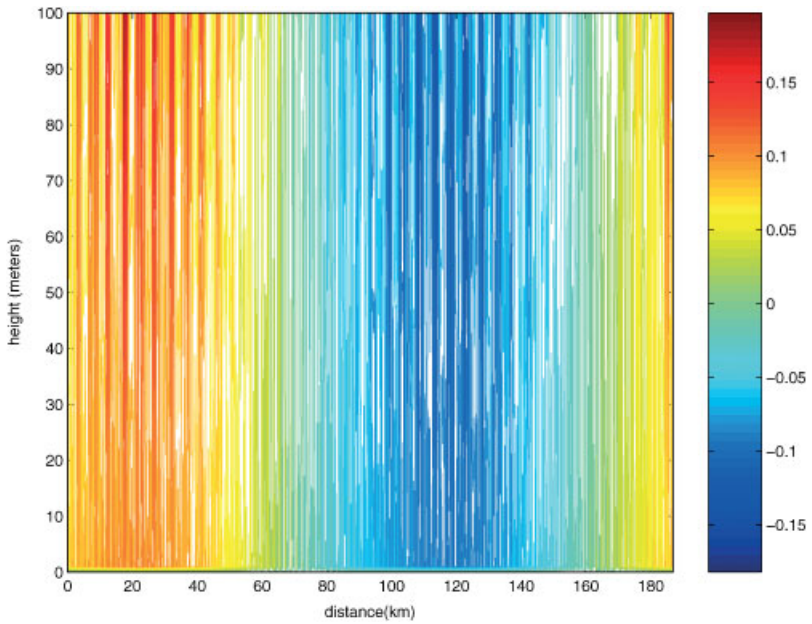

Plate 3. Contour plot of the vorticity as a function of the flight distance and height (simulation in the x–z plane).

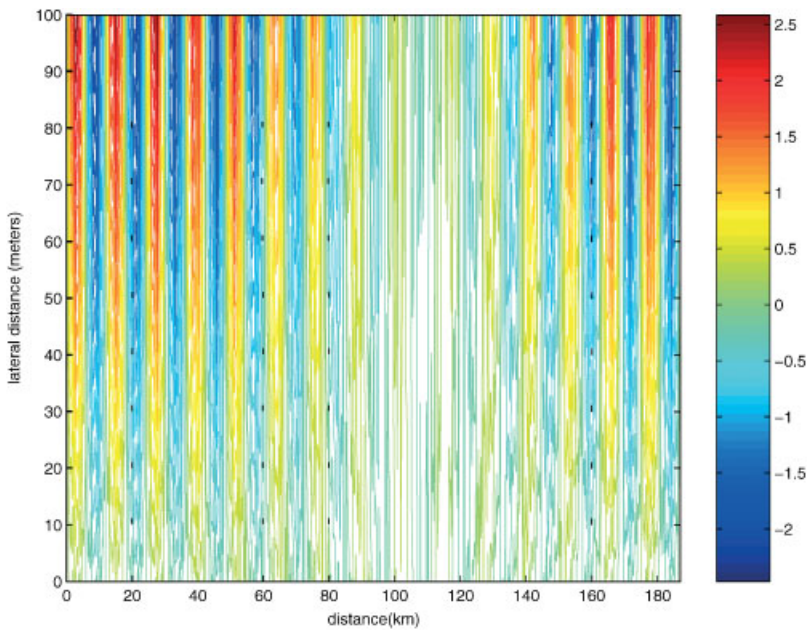

Plate 4. Contour plot of the temperature as a function of the flight and lateral distance (simulation in the x–y plane).

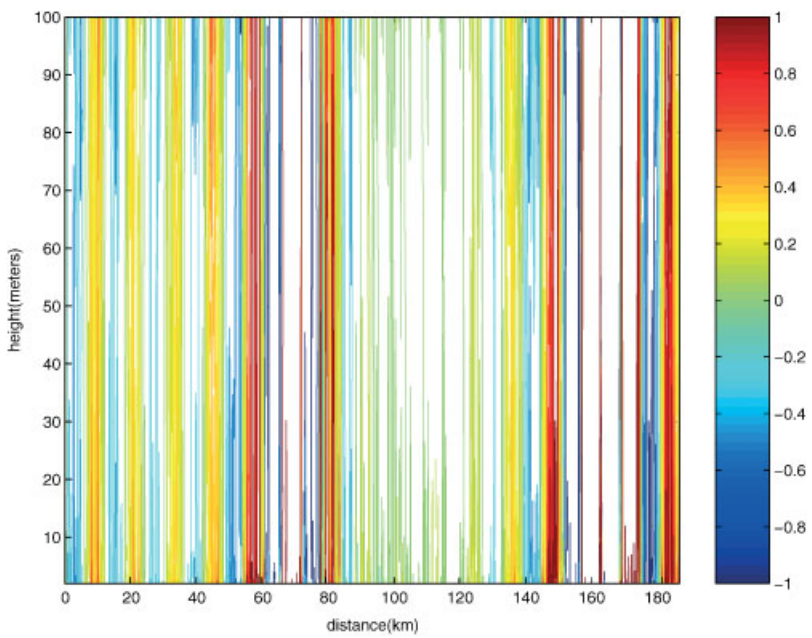

Plate 5. Contour plot of the Richardson number as a function of the flight distance and height (simulation in the x–z plane).

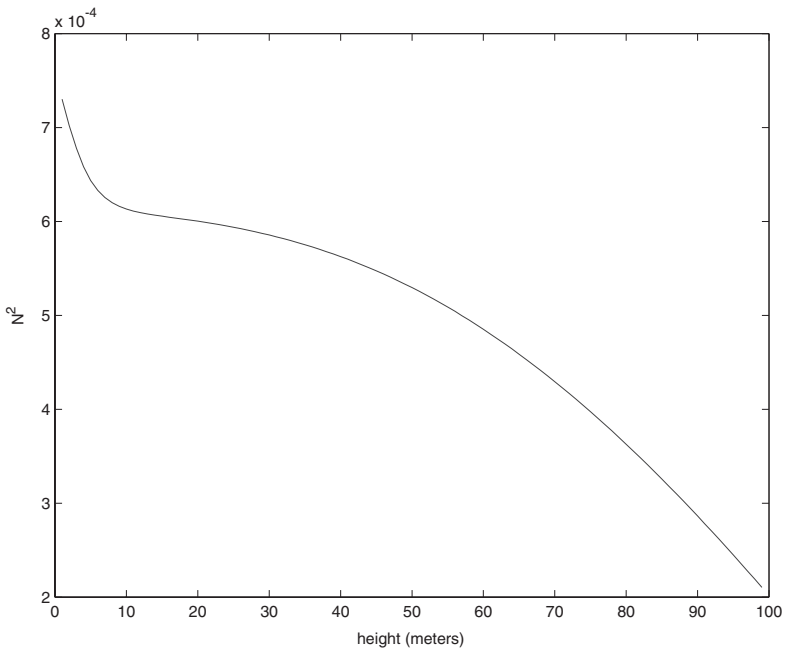

Figure 6. Plot of Brunt–Vaisala frequency (N^2) as a function of the height at flight distance of 60 km.

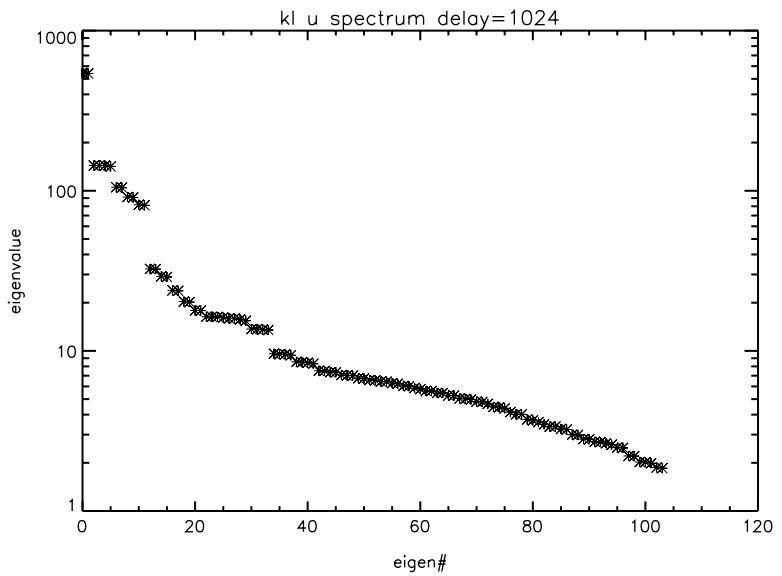

Figure 7. Karahunan–Loeve eigenvalue spectrum for u.

During the numerical integration the relative error in each step was set to 10^{-8} (floating point computations used 128 bit precision) with automatic-variable time step to satisfy this constraint.

Thus these two sources of error have a lesser impact on the solution than the errors which are due to the approximations made in order to be able to perform the two-dimensional cross section simulations. An estimation of the orders of the terms that were neglected leads to an error estimate in the range of 10–15% in the results.

6. CONCLUSIONS

The micro-structure of the flow (i.e. with resolutions of about 10 m) in the upper troposphere or the stratosphere cannot be obtained from numerical weather simulations where the grid spacing is of the order of 10 km. On the other hand initial data and boundary conditions for 3-D simulations of this flow in these resolutions are impossible to obtain by present means. The methodology presented in this paper (in spite of its obvious shortcomings) is perhaps the best one can devise to obtain at least some partial insight about this flow.

Using these cross-sectional simulations we have been able to obtain an estimate for the Richardson number and Brunt–Vaisala frequency along the airplane path (and as a function of the height from the plane). These results combined with spectral analysis can uncover important characteristics of the flow which are needed in many practical applications [8, 9].

APPENDIX A: K–L DECOMPOSITION

The statistical approach to turbulence splits the flow variables into a sum of mean flow, waves and turbulent residuals (see Equation (4.1)). To effect such a decomposition in our data we used the Karahunan–Loeve (K–L) decomposition algorithm (or PCA) which was used by many researchers (for a review see Reference [16]). Here we shall give only a brief overview of this algorithm within our context.

Let be given a time series X (of length N) of some geophysical variable. We first determine a time delay Δ for which the points in the series are decorrelated. Using Δ we create n copies of the original series

$$X(k), X(d+\Delta), \ldots, X(k+(n-1)\Delta)$$

(To create these one uses either periodicity or choose to consider shorter time-series). Then one computes the auto-covariance matrix $R=(R_{ij})$

$$R_{ij}=\sum_{k=1}^{N} X(k+i\Delta)X(k+j\Delta) \tag{A1}$$

Let $\lambda_0 > \lambda_1, \ldots, > \lambda_{n-1}$ be the eigenvalues of R with their corresponding eigenvectors

$$\phi^i=(\phi_0^i, \ldots, \phi_{n-1}^i), \quad i=0, \ldots, n-1$$

The original time series T can be reconstructed then as

$$X(j)=\sum_{k=0}^{n-1} a_k(j)\phi_0^k \tag{A2}$$

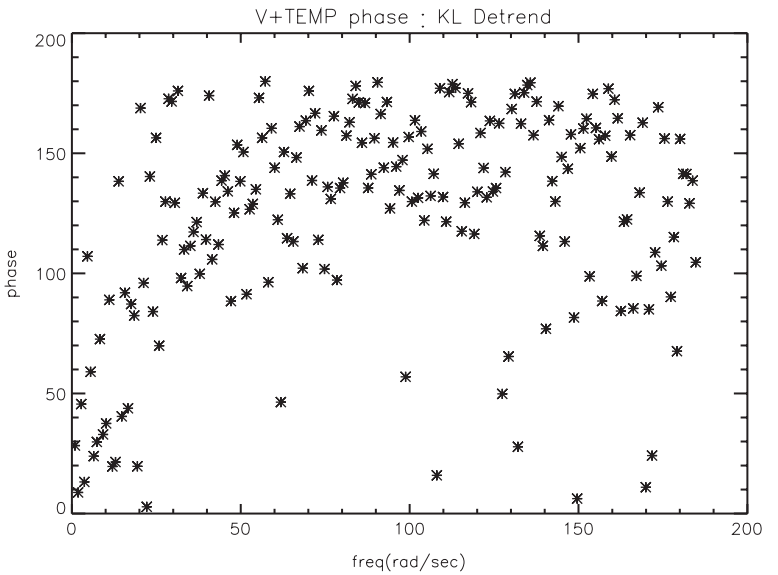

Figure A1. The phase between the detrended turbulent residuals of v and θ.

where

$$a_k(j) = \frac{1}{n} \sum_{i=0}^{n-1} X(j + i\Delta)\phi_i^k \tag{A3}$$

The essence of the K–L decomposition is based on the recognition that if a large spectral gap exists after the first m_1 eigenvalues of R then one can reconstruct the mean flow (or the large component (of the data by using only the first m_1 eigenfunctions in (A2). A recent refinement of this procedure due to Ghil *et al.* [16] is that the data corresponding to eigenvalues between $m_1 + 1$ and up to the point m_2 where they start to form a 'continuum' represent waves. The location of m_2 can be ascertained further by applying the tests devised by Axford [5] and Dewan [4] (see below).

Thus the original data can be decomposed into mean flow, waves and residuals (i.e. data corresponding to eigenvalues $m_2 + 1, \ldots, n - 1$ which we wish to interpret at least partly as turbulent residuals).

For the data under consideration we carried out this decomposition using a delay Δ of 1024 points for all the geophysical variables (a distance of about 1600 m). This delay was based on the Kennel's *et al.* mutual information test [18] and an estimate of 700–1000 m for the integral scale of the flow from the spectral plots (see Reference [10, pp. 174–176]).

The residuals of the time series which are reconstructed as

$$X^r(j) = \sum_{k=m_2+1}^{n-1} a_k(j)\phi_0^k \tag{A4}$$

contain (obviously) the measurement errors in the data. However to ascertain that they should be interpreted primarily as representing turbulence we utilize the tests devised by Axford [5]

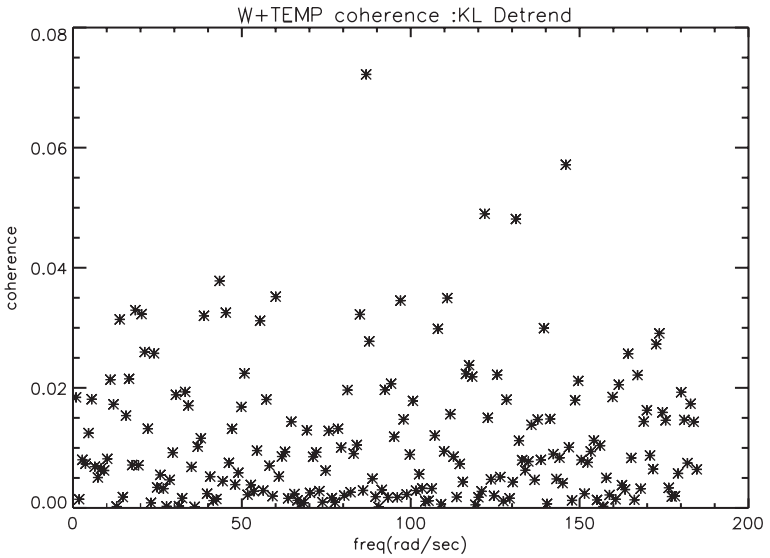

Figure A2. The coherence between the detrended turbulent residuals of w and θ.

and Dewan [4]. According to these tests turbulence data (at the same location) is characterized by low coherence between u, v, w and a phase close to zero or π between w and θ. (A phase close to $\pi/2$ is characteristic of waves).

These tests show that to a large extent the residuals that were obtained from the K–L decomposition represent actual turbulence. (Samples of the K–L decomposition spectrum, the coherence and phase are given in Figures 7, A1 and A2).

ACKNOWLEDGEMENTS

The author is deeply indebted to O. Cote of the U.S. Air-force Research Lab. and his team for access to the Egrett data and for many discussions regarding the issues involved in this research.

REFERENCES

1. Hipskind S, Gains S. Airborne Arctic Expedition, *NASA/VARP003*, May 1990.
2. Bacmeister JT, *et al.* Stratospheric horizontal wave number spectra of winds, potential temperature and atmospheric tracers observed by high altitude aircraft. *Journal of Geophysical Research* 1996; **101**:9441–9470.
3. Cote O, Dobosy R. Egrett measurements data in the upper troposphere during. Private communication, 1999–2000.
4. Dewan EM. On the nature of atmospheric waves and turbulence. *Radio Science* 1985; **20**:1301–1307.
5. Axford DN. Spectral analysis of aircraft observation of gravity waves. *Quarterly Journal of the Royal Meteorological Society* 1971; **97**:313–321.
6. Califano F. Turbulent transport in stably stratified fluids. *Revista del Nuovo Cimento* 1997; **20**:1–23.
7. Phillips OM. The generation of clear air turbulence by the degradation of internal waves. In *Atmospheric Turbulence and the Propagation of Radio Waves*, Nauka: Moscow, 1967; 130–138.
8. Cote O, Hacker JM, Crawford TL, Dobosy R. Clear Air Turbulence and Refractive Turbulence in the Upper Troposphere and Lower Stratosphere. Preprint.
9. Jumper GY, Beland RR. *Progress in the Understandings and Modeling of Atmospheric Optical Turbulence.* AIAA 2000–2355. *Proc. 31st AIAA Plasmadynamics and Lasers Conference*, *19–22 June 2000*, *Denver*, *CO*.

10. Panofsky HA, Dutton JS. *Atmospheric Turbulence*. Wiley: New York, 1984.
11. Valarde MG. Convective Instability. *Review of Modern Physics* 1977; **49**:581–623.
12. Schiesser WE. Method of lines solution of the Korteweg de Vries equation. *Computers and Mathematic with Applications* 1994; **28**:147–154.
13. Silebi CA, Schiesser WE. *Dynamic Modeling of Transport Process Systems*. Academic Press: New York, 1992.
14. Hindmarsh AC. ODEPACK, a systematized collection of ode solvers. In *Scientific Computing*, Stepleman RS *et al.* (eds), North-Holland: Amsterdam, 1983; 55–64.
15. Ghil M, Taricco C. *Advanced Spectral Analysis Methods*. In *Past and Present Variability of the Solar Terrestial System*, Cini Castagnoli G, Provenzale A (eds). Bologna and IOS press: Italiana di Fisica, 1997.
16. Penland C, Ghil M, Weickmann KM. Adaptive filtering and maximum entropy spectra, with application to changes in atmospheric angular momentum. *Journal of Geophysical Research* 1991; **96**:22659–22671.
17. http://www.netlib.org.
18. Kennel M, Brown R, Abarbanel H. Determining embedding dimension for phase space reconstruction using a geometrical construction. *Physical Review A* 1992; **45**:3403.

